ACADEMIC PRESS

Available online at www.sciencedirect.com
SCIENCE DIRECT®

Journal of Catalysis 214 (2003) 68–77

JOURNAL OF CATALYSIS

www.elsevier.com/locate/jcat

Catalytic isomerization of 2-pentene in H-ZSM-22—A DFT investigation

T. Demuth,[a,b,*] X. Rozanska,[c] L. Benco,[a] J. Hafner,[a] R.A. van Santen,[c] and H. Toulhoat[b]

[a] *Institut für Materialphysik, Universität Wien, Sensengasse 8, A-1090 Vienna, Austria*
[b] *Institut Français du Pétrole, 1 & 4 Avenue de Bois-Préau, F-92852, Rueil-Malmaison cedex, France*
[c] *Schuit Institute of Catalysis, Laboratory of Inorganic Chemistry and Catalysis, Eindhoven University of Technology, PO Box 513, NL-5600 MB Eindhoven, The Netherlands*

Received 20 May 2002; revised 7 September 2002; accepted 16 September 2002

Abstract

The skeletal isomerization of a 2-pentene molecule catalyzed by acidic ZSM-22 was investigated by ab initio DFT studies. Two different scenarios proposed in the literature were tested. First a reaction including an alkyl shift was considered: a methyl or ethyl group is detached from the carbenium ion chain and reattached at another site in the residual hydrocarbon chain. However, this mechanism is rather unlikely, since the alkyl ion is a high-energy species, so its detachment from the carbenium ion induces a high activation energy. We find that the more likely pathway for skeletal isomerization inside the channels of ZSM-22 involves the rearrangement of the carbenium ion into a protonated dimethylcyclopropane and implies the formation of relatively stable secondary carbenium ions as transient intermediates.

Keywords: Isomerization; Zeolites; Ab initio; Pentene; Carbenium; Alkoxy

1. Introduction

Within the context of catalysis by solid acids such as zeolites the skeletal isomerization of paraffins and olefins is an important reaction taking place in key processes of the refining industry [1]. Indeed, the conversion of light alkanes such as *n*-pentane and *n*-hexane into their branched isomers aims at improving the octane quality of gasoline. Conversion of *n*-butane into isobutane is important for increasing the availability of the latter hydrocarbon for alkylation or producing methyl-*t*-butyl ether. Skeletal isomerization of higher alkanes is the basis for the conversion of paraffin wax into lubricating base oils [2].

For the conversion of paraffins the combination of metals and zeolites in so-called "bifunctional" catalysts, which corresponds to a metallic catalyst dispersed over an acidic zeolite catalyst, is used. The metallic function catalyzes the dehydrogenation reactions that are required in the formation of alkenes. Noble metals such as Pt or Pd are mostly used for the dehydrogenation of alkanes. The acidic function (i.e., the Brønsted acid site of the zeolite) catalyzes the isomerization of alkenes into isoalkenes, which are finally hydrogenated back into isoalkanes on the metal [3,4].

If the catalyst contains a sufficient number of well-dispersed metallic clusters to allow equilibrium in the (de)hydrogenation step, the skeletal isomerization is the rate-determining step. Support for this mechanism is provided by the fact that the rate of *n*-pentene isomerization on a metal-free catalyst is essentially equal to that of the above overall reaction [5]. An additional benefit of the bifunctional catalyst is that the concentration of alkenes within the zeolite micropores remains low, which minimizes consecutive cracking or oligomerization. The latter reactions lead to coke formation and hence deactivate the catalysts.

2. Mechanisms of isomerization

Extensive experimental studies of skeletal isomerization have been performed and it was found that this reaction proceeds via either a mono- or a bimolecular reaction pathway [6–8]. The monomolecular mechanism is found to be more common with *n*-pentane and larger hydrocarbons in zeolites and also in sulfated zirconia. The bimolecular mechanism proceeds via a dimerization and cracking route and is observed to occur for the isomerization of *n*-butane, depending

* Corresponding author.
E-mail address: Thomas.Demuth@ifp.fr (T. Demuth).

0021-9517/03/$ – see front matter
doi:10.1016/S0021-9517(02)00074-X

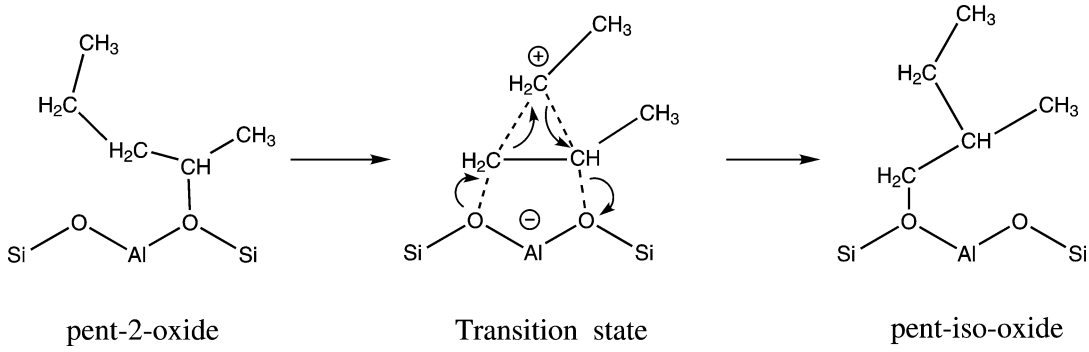

Fig. 1. Reaction mechanism of C_5 isomerization catalyzed by acidic zeolites via an alkyl (ethyl)shift.

on the type of catalyst and reaction conditions. For instance, in H-ferrierite the bimolecular mechanism was shown to occur on a fresh sample, whereas on the aged catalyst the monomolecular process became predominant [2].

The monomolecular isomerization in turn might occur via two possible reaction pathways, mediated either via a one-step alkyl shift mechanism or via a "protonated cyclopropane" intermediate reaction pathway. It is generally difficult to distinguish between these two cases on the basis of experimental data.

The reaction scheme for the isomerization of a pentene molecule via an ethyl shift catalyzed by an acid site is depicted in Fig. 1. The initial configuration shows a secondary alkoxy (covalent surface complex), namely a pent-2-oxide, which is the stable configuration of a chemisorbed pentenium ion. Next, an ethyl group is detached from the carbenium ion chain as an ethyl ion (methylcarbenium ion). The transition state complex is characterized as a triangular arrangement, the ethyl ion being in a bridge position between two carbon atoms. Finally, the ethyl ion is reattached at another place in the residual hydrocarbon chain. The final product is a primary isopentyl oxide. Generally, this simple mechanism is rather unlikely, since an alkyl ion is a high-energy species, so that its detachment from the carbenium ion chain would involve a prohibitively high activation energy [9]. Although within zeolites the carbenium and carbonium-ion-like transition states that are formed during a hydrocarbon reaction experience a stabilization due to the electrostatic potential of the anionic framework [10], it remains to be explored to which extent primary and secondary carbenium ions could be stabilized especially within small pore zeolites, like ZSM-22 as compared to the gas phase. Moreover, this degree of stabilization depends not only on the pore dimensions of the zeolite but also on the size of the adsorbed molecules. For chabazite, we have shown in a recent study that the order of the stability of primary and secondary carbenium-ion-like transition states is preserved [11] (i.e., the activation energy for protonation of a propylene inside acidic chabazite via a primary carbenium ion transition state is around 128 kJ/mol, for the formation of the more stable secondary transition state a barrier of just 56 kJ/mol was calculated).

The more likely mechanism for skeletal isomerization of the intermediate carbenium ion involves the rearrangement of the secondary carbenium ion into a protonated dialkylcyclopropane. This mechanism was originally proposed by Brouwer and Hogeveen [12] for skeletal isomerization in liquid superacids and later by Weitkamp [13] for isomerization in zeolites. The reaction mechanism is depicted in Fig. 2, path a. Starting from the same reactant alkoxy species, dimethylcyclopropane (in the following we will use the term DMCP) is formed by a proton backdonation from the hydrocarbon molecule to the zeolite, forming a Brønsted acid site. The intermediate configuration shows physisorbed dimethylcyclopropane interacting with the zeolite acid site. Afterward the ring is reopened by protonation; a different bond is broken, leading thus to a secondary pentyloxide. Only the more stable carbocation-like secondary transition states and intermediates are involved within this mechanism. Another possible scenario would be a transfer of a hydrogen atom within the ring of the cyclopropane (see Fig. 2, path b). This avoids the formation of the physisorbed DMCP intermediate. However, the mechanism for such a transfer within the DMCP adsorbed in a zeolite remains unclear.

A strong evidence for the protonated cyclopropane (PCP) isomerization mechanism is the fact that *n*-butane is not isomerized by superacids like $HSbF_6$ at room temperature, whereas *n*-pentane and *n*-hexane are rapidly converted into their isomers [2]. This can be understood, since for C_4 the rupture of only one bond in the cyclopropane ring would lead to the isobutane skeleton, but at the price of the formation of an energetically unfavorable primary carbenium ion. A cleavage of the two other bonds of the ring is possible, but will in both cases result in a secondary carbenium ion with a straight chain leading either to the original *n*-butane or to another C_4 molecule in which two carbon atoms have exchanged their position along the chain. Using ^{13}C-labeled *n*-butane, it is possible to detect that such an exchange indeed occurs [14].

Both cracking and isomerization are catalyzed by similar acid catalysts. Since skeletal isomerization requires a carbon chain of more than four atoms, whereas cracking needs at least seven atoms in the chain, pentanes and hexanes occupy a unique position in that they can be easily isomerized, but not easily cracked [2]. Indeed, highly selective isomerization

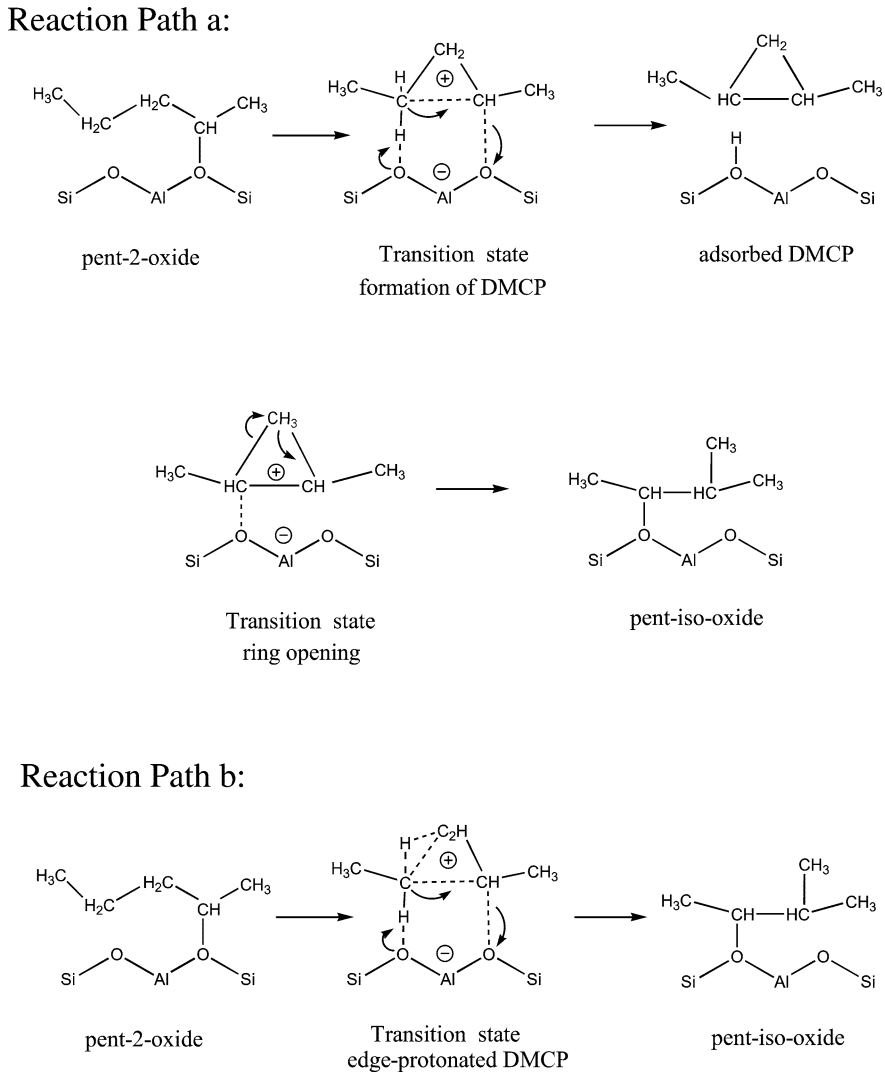

Fig. 2. Reaction mechanism of C_5 isomerization catalyzed by acidic zeolites via a dimethylcyclopropane intermediate (path a) or via an edge-protonated dimethylcyclopropane transition state (path b).

of C_5 and C_6 is easily achieved in practice. For higher alkanes, cracking may accompany isomerization, resulting in a lower selectivity for isomerization [15].

3. Structure of ZSM-22

In this paper we present a detailed study of the skeletal isomerization reaction of 2-pentene in acidic ZSM-22. This zeolite (which is isostructural to TON) is characterized by a one-dimensional channel system [16]. The main 10-membered ring channel, running parallel to the [001] direction, measures 5.5×4.5 Å. It has a framework consisting of 5-, 6-, and 10-rings. The structure contains ferrierite sheets of the type also found in ZSM-5 or ZSM-11 and sheets of 6-rings (see Fig. 3). However, the small channels do not allow molecules to enter or diffuse, so they are not considered as pores. All-silica ZSM-22 crystallizes in the orthorhombic space group *Cmcm* with lattice constants $a = 13.86$ Å, $b = 17.41$ Å, and $c = 5.04$ Å. This zeolite structure was chosen since ZSM-22 is a catalyst highly used for isomerization reactions [17]. Despite the fact that it was necessary to triple the primitive cell along the *c*-axis, in order to avoid adsorbate–adsorbate interactions between neighboring images, the total number of atoms ($N_{at} = 108$) within the supercell is still appropriate for electronic structure calculations based on periodic boundary conditions. One acid site per cell is present in the structure, leading to a Si/Al ratio of 35. A quantum chemical analysis of the isomerization reaction via alkyl shifts, using the cluster approach, was carried out in Refs. [18,19]. The pathway via the PCP was investigated by Frash et al. [20], again using the cluster approach. Boronat et al. have investigated the isomerization mechanism of linear butenes at zeolite clusters [21]. Our investigation is so far the first attempt to study an isomerization reaction of a linear alkene, taking the effects of the zeolite framework into account by the use of periodic boundary conditions.

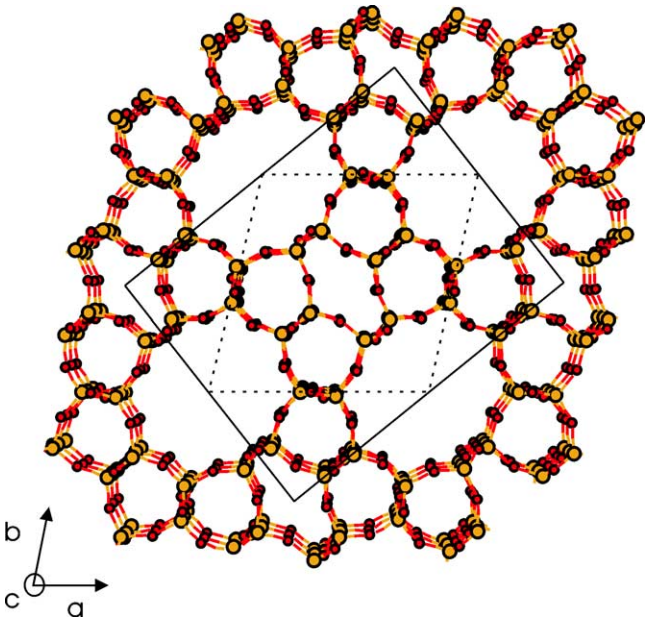

Fig. 3. Projection of the framework of ZSM-22 (TON) along the *c*-axis, presenting a view along the main channel (10 MR). The solid frame shows the conventional cell orthorhombic cell, the dashed frame the primitive unit cell.

4. Methodology

Ab initio total-energy calculations have been performed using the Vienna ab initio simulation package (VASP) [22,23]. VASP performs an iterative solution of the Kohn–Sham equations of density-functional theory (DFT), based on the minimization of the norm of the residual vector to each eigenstate and an efficient charge density mixing. For the exchange-correlation functional, gradient-corrected functionals in the form of the generalized gradient approximation (GGA) of Perdew and Wang 91 (PW91) have been used [24]. The calculations are performed in a plane-wave basis set, using the projector-augmented wave (PAW) method originally developed by Blöchl [25] and recently adapted by Kresse and Joubert [26]. A plane-wave cutoff of 400 eV was used in the calculations. Due to the large unit cells of zeolites, it is legitimate to restrict the Brillouin-zone sampling to the Γ-point, using a modest smearing of the eigenvalues to improve total-energy convergence. A conjugate-gradient algorithm was chosen for the structural relaxation. Except for the cell volume, which was fixed to the experimental value, all lattice constants and all internal parameters were allowed to relax.

For calculating reaction energy barriers the nudged elastic band method was used [27]. A series of images of the system along the reaction path is created and connected together with springs in this method. Force minimization is then applied, relaxing the images down the minimum energy path, making sure that they move only in the hyperplane perpendicular to the reaction path. The image showing maximum energy was afterwards optimized separately using a quasi-Newton algorithm till the forces acting on the ions were less then 0.07 eV/Å. The system that is finally obtained corresponds to an estimate of the transition state complex (i.e., maximum in energy with forces close to zero).

VASP has been successfully applied for studying structural and acidic properties of zeolites [28], adsorption phenomena [29], and hydrocarbon transformations within acidic zeolites [30].

Finally, we would like to underline the reliability of the calculated activation energies, despite the fact that within DFT calculations van der Waals (vdW) contributions are not explicitly taken into account. First of all, as in zeolites, the transition states are of an ionic nature, the electrostatic contributions to the activation energy are dominant, compared to distributions resulting from dispersive interactions. In order to estimate these dispersive contributions, we used a simple model, summing over all O_{zeo}–H_{mol} and O_{zeo}–C_{mol} distances and calculating the potential energy, using a 9–6 Lennard–Jones potential [31] assuming that the configuration is not changed due to the dispersive interaction. This procedure was applied to all minima and maxima along the reaction pathway. We found that, e.g., the vdW contribution for the physisorbed DMCP at H-ZSM-22 is around 55 kJ/mol. Rather similar values were calculated for the other configurations (largest difference around 7 kJ/mol). Hence, the vdW contribution only shifts the whole energy diagram to lower energies, and therefore maintains the relative energy differences as calculated by DFT.

5. Chemisorption of 2-pentene

We will start the investigation of the skeletal isomerization reaction pathway with the chemisorption of a 2-pentene molecule at acidic ZSM-22. The initial and final (de)hydrogenation steps of the hydroisomerization process will not be considered here for the following reasons. As mentioned before, these steps will presumably take place not at the Brønsted site but at a metallic site. Furthermore, the barriers for the (de)hydrogenation reactions are rather low, as indicated by the thermodynamic equilibrium between saturated and unsaturated hydrocarbons. The rate-limiting step of the hydroisomerization reaction is thus the transformation of the *n*-pentenium to the isopentenium as the step of the chemisorption of an alkene already occurs at room temperature [32].

The three most significant configurations along the minimum energy path of the chemisorption step are shown in Fig. 4. The reactant geometry corresponds to a weakly adsorbed 2-pentene at the acid site of ZSM-22. For the initial configuration the molecule was placed inside the main channel with the C2=C3 double bond parallel to the *c*-axis. Furthermore, the terminal C5 atom was rotated into the *cis*-position relative to the rest of the molecule as shown in Fig. 4. After the structural relaxation, two different H_{zeo}–C distances to the carbon atoms of the double bond are observed, viz., a rather short distance of 2.17 Å(C3) and a

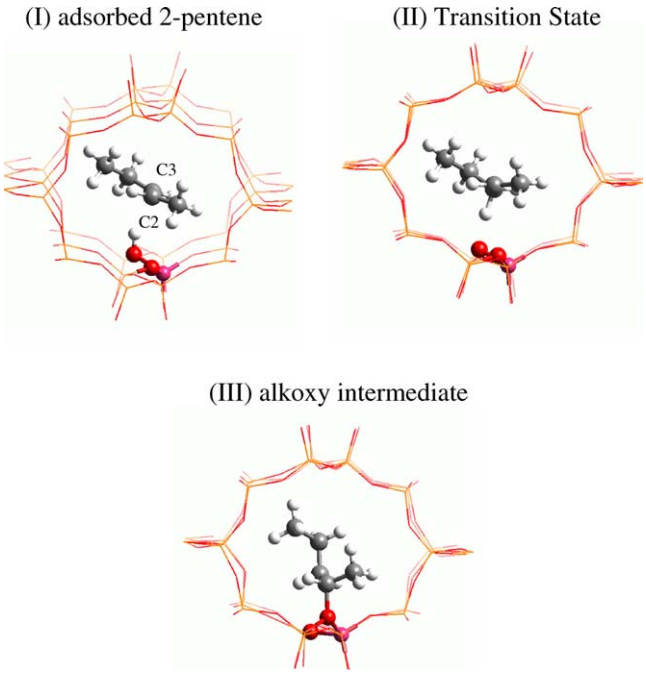

Fig. 4. Physisorbed, protonated, and chemisorbed 2-pentene at acidic ZSM-22.

longer distance to the C2 atom of around 2.70 Å. Hence, within this π-complex, the Coulomb interaction between the acidic proton and the molecule is rather asymmetric, due to steric constraints imposed by the small channel size of ZSM-22. This asymmetric interaction is also indicated by the differential charges, where a pronounced depletion of electron density occurs only for the π-orbitals of the more strongly interacting carbon atom (see Ref. [33]). The arrangement of the 2-pentene molecule inside the 10 membered-ring leads to quite short H–O_{zeo} distances, around 2.1 Å. The main structural parameters concerning the acid site are compiled in Table 1. The structural deformations of both the adsorbed molecule and the acid site compared to the adsorbed free structure are rather modest. The calculated adsorption energy of 2-pentene in H-ZSM-22 is 34 kJ/mol.

The geometry of the transition state shows an activated 2-pentene molecule, the acidic proton being transfered to the C3 carbon atom, leading thus to the formation of a secondary carbenium ion. The newly created C3–H covalent bond distance is around 1.20 Å. The hydrogen-bond length between the transfered proton and the framework oxygen atom is ∼ 1.66 Å. Due to the protonation the order of the former C2=C3 double bond changes and its length is increased to 1.41 Å; the neighboring C3–C4 single bond is enlarged to 1.54 Å and the C2–C1 bond decreases to 1.45 Å, in accordance with the bond-order conservation law [10]. Furthermore a slight torsional rotation of the $C1H_3$ group by 5° and of the $C4C5H_5$ ethyl group by 8° is observed. The structural deformations of the anionic zeolite framework are rather strong and not just localized to the vicinity of the AlO_4 tetrahedron. Both the Al–O(H) and Si–O(H) bond lengths (O(H) denotes the oxygen atom where the proton was previously attached, O(C) the oxygen where the alkoxy C–O bond with the molecule will be formed; see also Fig. 4) shrink, whereas the Al–O(C) distance increases, compared to the reactant configuration. Changes concerning the intertetrahedral angles are rather small (see Table 1). Except for one rather short H–O_{zeo} hydrogen bond of ∼ 2.21 Å, the mean distances between the charged molecule and the zeolite framework (H_{mol}–O_{zeo}) are around 2.5 Å.

Table 1
Main structural parameters (distances in Å, angles in °) of the zeolitic framework around the aluminum site for the physisorbed, transition state, and chemisorbed 2-pentene in ZSM-22

	Physisorbed	TS	Chemisorbed
Al–O(H)	1.890	1.784	1.726
Al–O(C)	1.709	1.742	1.899
Si–O(H)	1.696	1.612	1.591
Si–O(C)	1.593	1.599	1.693
Al–O(H)–Si	127.8	127.1	138.1
Al–O(C)–Si	133.3	134.1	122.7

The product geometry corresponds to a chemisorbed C_5 molecule, namely a pent-2-oxide alkoxy (see III, in Fig. 4). The C2–O bond length between the molecule and the zeolite is around 1.56 Å. Due to the chemisorption the Al–O(C) distance is decreased by 0.15 Å. Rather large angular changes are observed for both the Al–O(H)–Si and the Al–O(C)–Si by ∼ 10° compared to the values for the physisorbed geometry (see Table 1). It is important to mention that the covalent C2–O bond occurs at a different framework oxygen atom to that at which the acidic proton was initially attached. All molecular C–C bonds are in a range between 1.51 and 1.52 Å and can thus be considered as single bonds.

The energy difference between the final and the starting configuration was calculated to be 7 kJ/mol; the activation energy is 52 kJ/mol. Compared to the activation of propylene inside acidic ZSM-22 the barrier is ∼ 12 kJ/mol lower [34]. The transition state geometry of an activated propylene is very similar to that found for a 2-pentene. Nearly the same bond lengths were found for the former C=C double bond (1.41 Å) as well as for the newly created C–H bond (around 1.17 Å). A slightly larger value of about 1.8 Å was observed for the distance between the transferred proton and the zeolite oxygen atom. Also, for the geometry of the anionic zeolite framework, a similar distortion pattern was found. Hence the lower activation energy must be attributed to the higher degree of stabilization of the carbenium-ion-like transition state. Although for both propene and 2-pentene transition states, secondary carbenium-ion-like structures are created, the existence of the additional ethyl group could explain the larger stabilization and hence the lower barrier. Furthermore, also due to the small channel size of ZSM-22, the bulkier carbenium ion transition state, as in the case of 2-pentene, is better stabilized. Hence, it is expected that for zeolites with larger pores the differences in the activation energies for chemisorption of propene and 2-pentene will decrease.

6. Alkyl shift reaction

The methyl shift mechanism has been considered as the most obvious mechanism of several possible paths for the skeletal isomerization (e.g., for the monomolecular isomerization of *m*-xylene). However, quantum chemical cluster studies [19] have demonstrated that for aliphatic hydrocarbons ethyl shifts are possible as well as methyl shifts. The difference in the activation energies is negligible (around 4 kJ/mol). However, in small-pore zeolites methyl shifts are favored since an isomerization reaction via an ethyl shift would be sterically hindered. Here, we consider the skeletal isomerization via both ethyl and methyl shift pathways inside the main 10 MR. The initial reactant configuration of this reaction step is equal to the product configuration from the chemisorption step of a 2-pentene molecule, i.e., a chemisorbed pent-2-oxide. As it is seen in the reactant configuration (see Fig. 5), the alkoxy was arranged in a way favoring an ethyl shift reaction with the C3–C4 bond parallel to the *b*-axis. The transition state is also shown in Fig. 5; the corresponding geometrical parameters of the carbenium ion are compiled in Table 2. The geometry is best described by a quasi-triangular arrangement of three carbon atoms. The former C3–C4 bond of the linear reactant molecule is disrupted (distance at the TS around 1.77 Å) and a new bond at C2–C4 will be created (distance around 1.81 Å). The C2–C3 bond length of the C_3 hydrocarbon fragment shrinks to 1.39 Å. The neighboring C1–C2 distance is also decreased slightly to 1.48 Å. An increase to 1.54 Å is observed at the shifted ethyl ion (C4–C5).

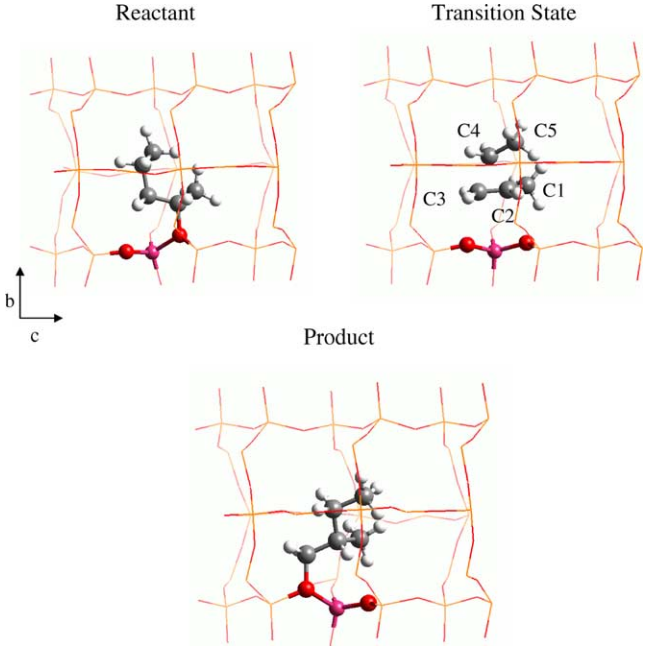

Fig. 5. Reactant, transition state, and product configuration for the isomerization via an ethyl shift (the atoms of the reacting molecule as well as the closest aluminum and oxygen framework atoms are highlighted).

Table 2
Structural parameters (distances in Å, angles in °) for the transition state via an ethyl shift

C1–C2	1.485	C2–C3	1.391
C3–C4	1.771	C2–C4	1.814
C4–C5	1.548		
C3–H	1.088	C4–H	1.096
C2–C3–C4	70	C3–C2–C4	65
C3–C4–C2	45	C1–C2–C3	128
C3–O	2.552	C2–O	2.673

For notation see Fig. 5.

The triangular arrangement is also indicated by nearly equal C2–C3–C4 and C3–C2–C4 angles (see Table 2). Concerning distances between carbon atoms of the carbenium ion and framework oxygen atoms, the former covalent C2–O bond of the initial alkoxy is broken, showing an increased distance of 2.67 Å. An even smaller C–O distance of 2.55 Å was found for the C3 atom. This already indicates that for the final state the C3 atom will form a covalent bond with this oxygen atom. The transition state is furthermore characterized by four nearly equal Al–O bond lengths (∼ 1.75 Å). The same applies also to the Al–O–Si intertetrahedral bond angles (∼ 133°).

The final product geometry corresponds to an adsorbed branched alkoxy complex (see Fig. 5). The C3–O distance is around 1.54 Å. The molecular C–C distances are around 1.52 Å, one of them being slightly larger (1.53 Å). This longer C2–C4 bond length corresponds to the newly created bond of the attached ethyl group at the residual hydrocarbon chain. C–H bonds are around 1.09 Å. Typical H–O_{zeo} hydrogen bond lengths are in the range between 2.1 and 2.3 Å. As for the initial alkoxy configuration, a pronounced decrease of the Al–O(C)–Si intertetrahedral angle to 121° was observed. Thus the chemical bonding at the oxygen atom is best explained by sp^2 hybrid orbitals, whereas for the carbon atom the bonding occurs via sp^3 orbitals. The Al–O(C) distance in the final configuration is around 1.88 Å; the neighboring Si–O(C) bond length is 1.69 Å.

The energy difference between the carbenium-ion transition state and the initial secondary alkoxy was calculated to be $E_{act} \sim 180$ kJ/mol. Between the reactant and product configurations the energy difference was found to be around 58 kJ/mol, the initial configuration being energetically more stable. The reason for that rather large difference in energy between the reactant and the product can be explained by steric constraints. In the product configuration (primary alkoxy) the terminal methyl group of the shifted ethyl ion ($C5H_3$; see Fig. 5) is in rather close contact with framework oxygen atoms (average O_{zeo}–H_{methyl} distances around 1.7 Å). Such small distances are not present in the reactant configuration (secondary alkoxy). Furthermore, the different stability level of a primary versus secondary alkoxy also has to be taken into account, although it was shown for propylene chemisorption in zeolites that the formation of a

primary alkoxy complex is by only ∼ 7 kJ/mol less favorable compared to the formation of a secondary one [19].

As mentioned before, the reactant configuration shows a more stable secondary alkoxy, whereas the branched alkoxy is of primary character. In order for the product configuration to correspond to a secondary alkoxy complex as well, a hydride-transfer along the hydrocarbon chain of the carbenium ion is necessary. If one assumes a hydride-shift from the C2 to the C3 carbon atom, even a tertiary alkoxy can be formed. Recently, we have shown by means of ab initio molecular dynamics at high temperatures that hydride shifts occur frequently along charged hydrocarbons adsorbed within zeolites [35]. Hence, the corresponding barriers are expected to be small.

An isomerization via a methyl shift reaction was studied as well. For the transition state configuration, which is described by a triangular arrangement of a methyl ion and the residual hydrocarbon chain, the distance between the two carbon atoms where the bond is broken is around 1.83 Å, and a distance of 1.97 Å was found between the C atoms, where a bond will be formed in the product configuration. These distances are slightly larger than those for the ethyl shift TS. In total this leads to a less symmetrical configuration. All other C–C and C–H distances, as well as the molecular angles, are very close to the values found for the transition state via an ethyl shift. The longer distances are caused by the availability of more void space for a methyl ion than for the larger and bulkier ethyl ion. Accordingly, the calculated barrier is even higher (by ∼ 15 kJ/mol) with respect to the activation energy for the ethyl shift. The main reason for this difference is that the methyl ion is less stable in energy compared to an ethyl ion.

Finally, it is important to mention the bifunctional nature of the active site. The Brønsted part is responsible for the protonation of the olefin, whereas the interaction with the neighboring basic oxygen converts the resulting carbenium ion into a surface alkoxy.

7. Reaction via formation of DMCP

Since it was shown in the previous section that the mechanism for the skeletal isomerization via an alkyl shift exhibits a rather high barrier due to the formation of a primary carbenium ion, we investigated also the proposed mechanism via a protonated dimethylcyclopropane (DMCP) intermediate. The basic steps for this mechanism have already been briefly outlined (see Fig. 2). For further details we refer to Ref. [2].

The starting configuration corresponds again to a linear unbranched surface alkoxy (structural parameters are compiled in Table 3). In order to create a DMCP intermediate the covalent alkoxy C–O_{zeo} bond is disrupted in a first step. This produces a protonized molecule representing the first transition state (TS 1), shown in Fig. 6. Upon desorption the former covalent C2–O bond length is increased to 2.64 Å in the TS and the intertetrahedral Si–O–Al angle is increased from 115° to 131°.

Table 3
Structural parameters (bond lengths in Å, angles in °) for the initial, final, transition states and intermediate configurations for the reaction pathway via a protonated DMCP

	Initial	TS 1	Int.	TS 2	Ads. DMCP	TS 3	Final
C1–C2	1.515	1.450	1.472	1.501	1.509	1.482	1.513
C2–C3	1.520	1.446	1.417	1.447	1.504	1.819	
C3–C4	1.531	1.551	1.621	1.558	1.510	1.645	1.531
C4–C5	1.523	1.521	1.523	1.521	1.502	1.511	1.510
C2–C4		2.630	1.944	1.667	1.516	1.414	1.526
C1–C2–C3	115.4	126.4	124.0	119.0	117.2	109.5	
C2–C3–C4	118.4	122.0	78.6	67.3	60.1	49.8	110.2
C3–C4–C5	113.3	113.0	110.2	110.6	118.1	112.0	109.6
C–O_{zeo}	1.55	2.64	3.21	3.11	3.37	4.23	1.56
H–O_{zeo}		2.29	2.16	2.43	2.33	2.36	

For notation see Fig. 6.

The two C–C distances of the secondary carbenium ion next to the charged carbon atom (C2) are around 1.45 Å, the remaining two bond lengths being C3–C4 1.55 Å and C4–C5 1.52 Å (see Table 3). All C–H distances are around 1.09 Å. Shortest distances between the molecule and the zeolite lattice (i.e., H–O_{zeo} hydrogen bonds) are around 2.29 Å. The activation energy for this step was calculated to be E_{act} ∼ 58 kJ/mol. Since this reaction step is nearly the same as that for the reverse reaction of the initial chemisorption of the 2-pentene (i.e., in both cases a desorption of an alkoxy species occurs), the calculated barriers are very similar (E_{act} around 59 versus 58 kJ/mol).

The next important configuration along the reaction energy path corresponds to a stable charged intermediate (see Fig. 6 (Int)). Starting from the TS 1 configuration the C2–C4 distance is decreased to create a cyclic structure. The C2–C4 distance is around 2.63 Å in the starting alkoxy and TS 1 geometry and around 1.94 Å in the intermediate configuration. Accordingly, the C2–C3–C4 angle is decreased by approximately 43° to 78°. Concerning the remaining C–C bond lengths, the C3–C4 distance is enhanced to 1.62 Å, whereas a decrease to 1.41 Å was found for the C2–C3 bond

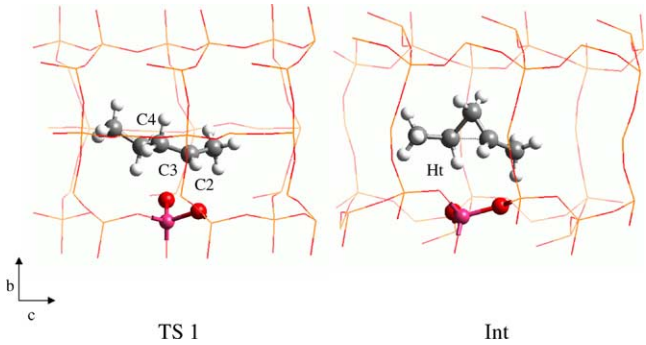

Fig. 6. Transition state geometry (TS 1) for breaking the alkoxy C–O_{zeo} bond (left) and the optimized geometry of the corner protonated DMCP intermediate (right).

length. The closest distance between a hydrogen atom of the carbenium ion and an oxygen atom of the surrounding lattice is about 2.16 Å. It is precisely this hydrogen (Ht, see Fig. 6 (Int)) which will be reattached to the zeolite in the following reaction step. It is important to emphasize that this configuration does not correspond to a saddle point along the minimum energy path, but to a stable intermediate. This was also confirmed by an analysis of the vibrational spectrum (based on a numerical evaluation of the force constants) since no negative eigenvalue and thus no imaginary frequency was found. This is an interesting result since normally alkyl carbenium ion structures exist just as transition states within zeolite-catalyzed reactions and not as stable intermediates [18]. The reason for the existence of such a carbenium ion might be related to the high stability of that species inside the framework of the zeolite. The positive charge at the C2 atom is stabilized not only via the neighboring carbon atoms (C1 and C3), but additionally via the C4 atom (C2–C4 distance around 1.94 Å). Hence, this charged molecule is closer to a tertiary carbenium ion than to a secondary one. The increase in stabilization as a function of the C–C distance is also indicated along this part of potential energy surface. Starting from the TS 1 the corresponding configuration becomes more stable as the distance decreases till the intermediate configuration is formed. Furthermore, the small channel size of ZSM-22 also contributes to the stabilization of such a species. However, it remains to be explored whether such an intermediate could also exist in large-pore zeolites. This intermediate configuration is by ~ 24 kJ/mol less stable with respect to the initial alkoxy configuration. A further decrease of the C2–C4 distance would lead to the formation of a "corner-protonated" DMCP; however, within a zeolite, the closing of the C2C3C4 triangle induces proton backdonation from the carbenium ion to the zeolite, creating a Brønsted acid site. Simultaneously, the C2–C4 distance is further decreased, leading finally to a neutral DMCP molecule which is weakly physisorbed at the acid site. Both the transition state (TS 2) geometry and the final physisorbed configuration are depicted in Fig. 7.

In the transition state for proton backdonation (TS 2), the transferred proton is nearly located between the donating C4 carbon atom (C4–H distance ~ 1.34 Å) and a framework oxygen atom (H–O_{zeo} ~ 1.41 Å). The C2–C4 distance is around 1.66 Å. The geometrical arrangement of the hydrocarbon is already quite close to that of a neutral DMCP molecule (see Table 3). Concerning the zeolite framework the Al–O–Si intertetrahedral angle is decreased by 10° to 128° with respect to the intermediate configuration, indicating a weak Coulomb interaction between the proton and the anionic zeolite framework.

The final configuration, corresponding to a physisorbed DMCP, is depicted in the right part of Fig. 7. The adsorption is realized via weak hydrogen bonds between the acidic proton and two carbon atoms of the cyclic ring (distances around 2.82 Å). The weak interaction is also indicated by the low value of just 8 kJ/mol for the heat of adsorption. No structural distortions of the DMCP molecule were observed. Hence, the molecule is nearly unbound to the zeolite. This configuration is by ~ 15 kJ/mol less stable than the initial reactant configuration.

Finally, the C3 site becomes protonated in order to finish the isomerization reaction. This can be achieved by rotating the DMCP molecule by approximately 90° along the *c*-axis (see Fig. 8) The activation of the molecule at the C2 or C4 atom would lead back to a linear carbenium ion, whereas only a protonation at the C3 carbon atom leads to a branched molecule. Since the interaction of the DMCP with the zeolite is very weak, the rotational barrier is expected to be small. To avoid the formation of an overcoordinated C-atom (and hence of a carbonium ion) simultaneously with the proton transfer, the C2–C3 bond is broken (breaking of the other C3–C4 carbon bond would be possible as well, leading also to a branched carbenium ion).

The final transition-state configuration for the reprotonation step is shown in Fig. 8. The Brønsted proton is already transferred back from the acid site and binds covalently to the C3 carbon atom. The distance between the zeolitic oxygen atom and the transfered proton is around 1.80 Å. Moreover, it is seen that the C2–C3 bond is broken (distance around 1.81 Å). The C3–C4 bond length is around 1.64 Å, the C2–C4 around 1.41 Å. The Al–O–Si angle is enlarged to $\sim 140°$.

Finally, a rerotation of the molecule occurs and via the C2 atom, where the positive charge is located, a secondary

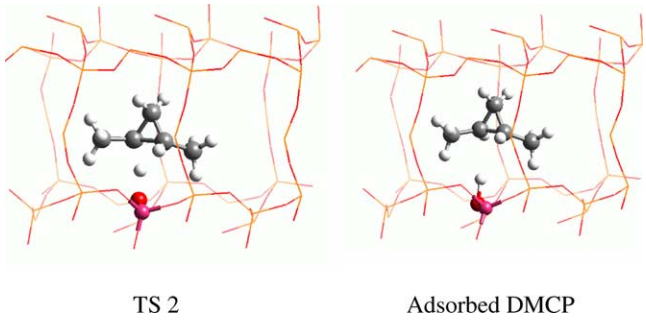

Fig. 7. Transition state geometry (TS 2) for the proton backdonation (left) and physisorbed complex (right).

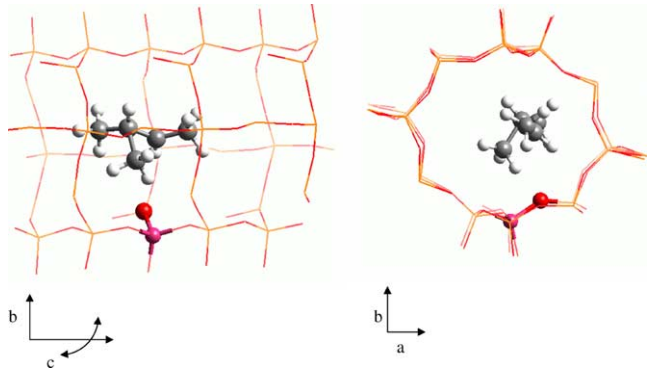

Fig. 8. Transition state geometry (TS 3) for the reprotonation and ring-opening (left: side view, right: top view).

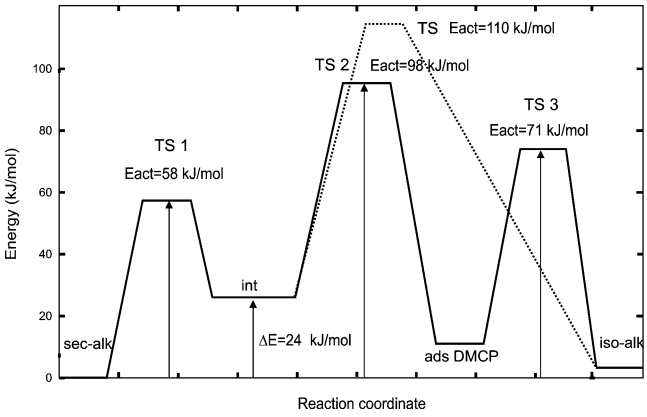

Fig. 9. Reaction energy diagram for the isomerization via a DMCP intermediate (solid lines), showing also the energy barrier for the pathway via the intramolecular hydrogen shift (dashed lines).

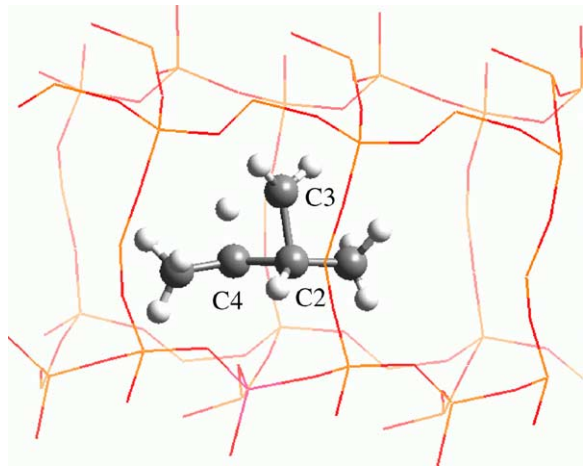

Fig. 10. Transition state geometry for the hydrogen jump from C4 to C3 (edge-protonated DMCP).

alkoxy complex is formed which corresponds to the product configuration in the final step.

The complete reaction pathway is depicted in Fig. 9. The overall reaction, starting from a linear alkoxy to a monobranched one, involves in total three transition states and two intermediate configurations. The highest barrier of ~ 98 kJ/mol was found for the proton backdonation (see TS 2). For the ringopening via the reprotonation of the DMCP molecule, an activation energy of 71 kJ/mol was calculated. Compared to the pathway via the ethyl shift the barriers found for this mechanisms are much smaller. Note that only secondary carbenium ions are involved within this mechanism.

8. Hydrogen transfer via an edge-protonated DMCP

As we have shown in the previous section, the reaction mechanism via a protonated DMCP should be favored, compared to the alkyl shift pathway. However, this pathway is characterized by a rather complicated series of molecular rotations of the DMCP molecule. Moreover, since the DMCP molecule is only weakly physisorbed inside the zeolite, it should potentially be detected in experimental studies, which is not the case. Hence it appears to be reasonable to find an alternative pathway, which avoids the occurrence of the physisorbed neutral DMCP intermediate. For such a pathway the initial steps, breaking the covalent C–O alkoxy bond (see TS 1, Fig. 6) and the formation of a stable protonated DMCP species (see Int, Fig. 6) are the same as described previously. However, within this mechanism no proton backdonation from the molecule to the zeolite occurs, but a hydrogen atom which is located at the C4 atom migrates to the C3 carbon atom (see Fig. 2, path b). This intramolecular transfer is realized via the formation of an "edge-protonated" DMCP (see the transition state configuration shown in Fig. 10). It is seen that the transferred hydrogen atom is located between the C3 and C4 atom. The distance to the latter is slightly smaller (C4–H ~ 1.21 Å, C3–H ~ 1.36 Å). The former C3–C4 bond is strongly elongated in the TS geometry, indicated by a large distance of 1.73 Å; the C2–C3 bond length is around 1.44 Å. The formation of an edge-protonated CP species (with an elongation of the protonated C–C edge) was also shown to be energetically only very slightly disfavored (by only 5.6 kJ/mol) for the gas-phase $C_3H_7^+$ compared to the corner-protonated species (see Ref. [36]).

As soon as the proton binds to the C3 carbon atom, either the C3–C2 or the C3–C4 bond is broken. Hence, the final product will always correspond to a monobranched alkoxy complex. Moreover, no rotation and no reprotonation step is necessary within this pathway. As mentioned before, the starting configuration corresponds to the stable protonated DMCP intermediate.

The charged molecule again binds as an alkoxy complex to the zeolite wall in the final step. The barrier for the proton jump was calculated to be 110 kJ/mol with respect to the initial linear alkoxy complex (see Fig. 9). Since this energy is just 12 kJ/mol larger than that for the previous pathway, we conclude that the two pathways are competitive. The calculation of reaction rates constants and rates might give further insight into which mechanism is more probable depending on the temperature, taking also the different amount of entropic contribution to the preexponential induced by the various rotations of the DMCP within the first pathway into account.

9. Conclusions

In this paper we have investigated the skeletal isomerization of a 2-pentene molecule catalyzed by acidic ZSM-22. The olefin is chemisorbed at a zeolite oxygen atom, leading to a surface alkoxy product complex, in the first step. The barrier for this step is rather low (E_{act} is around 50 kJ/mol). Three different mechanisms for the actual isomerization have been studied.

In the first, the transformation occurs via an alkyl shift reaction. A terminal methyl or ethyl ion is detached from the molecule and reattached at a different carbon atom of the residual hydrocarbon chain. The corresponding transition

state is characterized by a regular triangular arrangement of the carbenium ion. The barrier for this pathway is calculated to be $E_{act} = 180$ kJ/mol (ethyl shift). For the isomerization via a methyl shift an even higher barrier of 195 kJ/mol is found. This difference in activation energy between the methyl and ethyl shifts is correlated with the relative energy stability of the carbenium ion being involved in the transition state structure.

The second pathway occurs via a protonated cyclic intermediate. The overall mechanism is rather complex, involving three transition states and two intermediates (a secondary carbenium ion and a neutral physisorbed DMCP). The drawback of this reaction pathway is that a direct reprotonation of the CH_2 corner of the cycle, leading to the ring-opening and the chemisorption of the resulting branched carbenium ion, involves a rather complex sequence of molecular rotations. We have shown that an alternative scenario via an edge-protonated species leads to a slightly higher barrier (by just 12 kJ/mol) and might be preferred for kinetic reasons. It is also important to emphasize that the edge-protonated alkyl cyclopropanes are often considered in isomerization and cracking reactions. These reaction pathways via the DMCP have a much lower E_{act} than those which involve alkyl shifts (E_{act} around 100 kJ/mol versus 180 kJ/mol). Due to that rather large energy difference the alkyl shift pathway must be discarded.

The calculated activation energy for the skeletal isomerization has to be compared with the available experimental data, which show a rather large scattering. The experimental value for the activation energy for *n*-hexane hydroisomerization in ZSM-22 was measured at 240 °C to be 106 kJ/mol, assuming for the rate limiting step the isomerization of a linear alkoxy to a branched one [37]. For the isomerization of *n*-pentane in Pt/H-MOR even lower barriers, between 106 and 52 kJ/mol in different temperature ranges, were reported [6].

So far we have estimated the barriers as the energy differences between the starting pent-2-oxide and the several transition states (see Fig. 9). Due the existence of the stable intermediate (see Fig. 6, Int), the following activation energies should be calculated with respect to this species rather than to the initial alkoxy. The resulting barriers are thus around 74 kJ/mol (DMCP pathway via the H^+ back-donation) and 96 kJ/mol (pathway via the H-shift along the DMCP), respectively. However, this is only valid if this intermediate is thermodynamically stable. Hence, we conclude that a direct comparison with experimental activation energies for reaction pathways as presented here could be ambiguous. For this purpose rather rates or rate constants should be used.

Acknowledgments

This work has been performed within the Groupement de Recherche Européen (GdR-E) “Dynamique moléculaire quantique appliquée à la catalyse,” supported by the Centre National de la Recherche Scientifique (CNRS), the Institut Français du Pétrole (IFP), and TotalFinaElf. We thank I.D.R.I.S. (Orsay) and the Technical University of Vienna for the generously allocated computer time. Fruitful discussions with Pascal Raybaud and Christian Marcilly from IFP are gratefully acknowledged.

References

[1] B.C. Gates, Catalytic Chemistry, Wiley, New York, 1992.
[2] S.T. Sie, in: G. Ertl, H. Knözinger, J. Weitkamp (Eds.), Handbook of Heterogenous Catalysis, Vol. 4, VCH, Weinheim, 1997, p. 1998.
[3] P.B. Weisz, Adv. Catal. 13 (1962) 137.
[4] J. Weitkamp, H.J. Schultz, J. Catal. 29 (1973) 361.
[5] R.A. Van Santen, J.W. Niemantsverdriet, Chemical Kinetics and Catalysis, Plenum, New York/London, 1995.
[6] H. Liu, G.D. Lei, W.M.H. Sachtler, Appl. Catal. A 137 (1996) 167.
[7] M.A. Asensi, A. Corma, A. Martinez, J. Catal. 158 (1996) 561.
[8] K. Chao, H. Wu, L. Leu, J. Catal. 157 (1995) 289.
[9] L. Bell, Oil Gas 11 (1994) 65.
[10] R.A. Van Santen, G. Kramer, Chem. Rev. 95 (1995) 637.
[11] X. Rozanska, T. Demuth, F. Hutschka, J. Hafner, R.A. van Santen, J. Phys. Chem. 106 (2002) 3248.
[12] D.M. Brouwer, H. Hogeveen, Prog. Phys. Org. Chem. 9 (1972) 179.
[13] J. Weitkamp, Ind. Eng. Chem. Prod. Res. Dev. 21 (1982) 550.
[14] D.M. Brouwer, J.M. Oelderik, Rec. Trav. Chim. Pays Bas 87 (1968) 721.
[15] P. Raybaud, A. Patrigeon, H. Toulhoat, J. Catal. 197 (2001) 98.
[16] G.T. Kokotailo, J.L. Schlenker, F.G. Dwyer, E.W. Valyocsik, Zeolites 5 (1985) 349.
[17] M.A. Asensi, A. Corma, A. Martinez, M. Derewinski, J. Krysciak, S.S. Tamhankar, Appl. Catal. A 174 (1998) 163.
[18] V.B. Kazansky, Catal. Today 51 (1999) 419.
[19] A.M. Rigby, M.V. Frash, J. Mol. Catal. A 126 (1997) 61.
[20] M.V. Frash, V.B. Kazansky, A.M. Rigby, R.A. Van Santen, J. Phys. Chem. 101 (1997) 5346.
[21] M. Boronat, P. Viruela, A. Corma, J. Phys. Chem. 102 (1998) 982.
[22] G. Kresse, J. Hafner, Phys. Rev. B 48 (1993) 13115.
[23] G. Kresse, J. Hafner, Phys. Rev. B 49 (1994) 14251.
[24] J.P. Perdew, J.A. Chevary, S.H. Vosko, K.A. Jackson, M.R. Pedersen, D.J. Singh, C. Fiolhais, Phys. Rev. B 46 (1992) 6671.
[25] P. Blöchl, Phys. Rev. B 50 (1994) 17953.
[26] G. Kresse, D. Joubert, Phys. Rev. B 59 (1999) 1758.
[27] G. Mills, H. Jonsson, G.K. Schenter, Surf. Sci. 324 (1995) 305.
[28] T. Demuth, J. Hafner, L. Benco, H. Toulhoat, J. Phys. Chem. 104 (2000) 4593.
[29] L. Benco, T. Demuth, J. Hafner, F. Hutschka, Chem. Phys. Lett. 324 (2000) 373.
[30] X. Rozanska, R.A. Van Santen, F. Hutschka, J. Hafner, J. Am. Chem. Soc. 123 (2001) 7655.
[31] H. Sun, J. Phys. Chem. 102 (1998) 7338.
[32] E.G. Derouane, H. He, S.B.D.-A. Hamid, I. Ivanova, Catal. Lett. 58 (1999) 1.
[33] T. Demuth, L. Benco, J. Hafner, H. Toulhoat, F. Hutschka, J. Phys. Chem. 114 (2001) 3703.
[34] T. Demuth, X. Rozanska, L. Benco, J. Hafner, H. Toulhoat, J. Chem. Phys., in preparation.
[35] L. Benco, T. Demuth, J. Hafner, F. Hutschka, H. Toulhoat, J. Catal. 205 (2002) 147.
[36] W. Koch, B. Liu, J. Am. Chem. Soc. 111 (1989) 3479.
[37] R.A. Van Santen, F.J.M.M. De Gauw, Stud. Surf. Sci. Catal. 130 (2000) 127.